RSC Advances

PAPER

View Article Online
View Journal | View Issue

Cite this: *RSC Adv.*, 2015, **5**, 86564

A new and facile way to fabricate catalytically active block copolymer/Au nanoparticle multilayer thin films at the air/liquid interface

Qian Wang,[a] Xingjuan Zhao,[a] Yong-Ill Lee[b] and Hong-Guo Liu*[a]

Received 14th August 2015
Accepted 7th October 2015

DOI: 10.1039/c5ra16370f

www.rsc.org/advances

A composite polymer/Au nanoparticle multilayer film was fabricated at the air/liquid interface through a new and facile self-assembly and adsorption process. A planar liquid/liquid interface was formed at first by using a DMF/$CHCl_3$ mixed solution of polybutadiene-*block*-poly(4-vinylpyridine) (PB-*b*-P4VP) as the lower phase and a $HAuCl_4$ aqueous solution as the upper phase. The PB-*b*-P4VP molecules self-organized into disk-like micelles in the mixed organic phase. Because DMF is miscible with water, DMF carried the block copolymer molecules and micelles into the upper aqueous phase, and then diffused into the $HAuCl_4$ aqueous solution, leading to further self-assembly of the polymer molecules with the inorganic species and the formation of larger sheet aggregates. These aggregates further adsorbed at the air/liquid interface, resulting in the formation of the multilayer composite film. Most $AuCl_4^-$ ions were reduced by DMF during this process, and numerous Au nanoparticles were generated and embedded in the composite film. This film exhibited unique heterogeneous catalytic properties due to its unique multilayer structure.

Introduction

Amphiphilic block copolymers that contain separate hydrophobic and hydrophilic portions exhibit abundant self-assembly behavior in solutions,[1,2] as thin films,[3,4] and at air/water interfaces[5,6] due to their micellization and microphase separation properties. Thus, a series of ordered molecular assemblies, including spherical, cylindrical, rod, and disc-like micelles, vesicles, large compound micelles, nanotubes, and many other structures, have been obtained in solutions,[7–11] whereas ordered arrays of micelles or reverse micelles,[12] and parallel or perpendicular cylinders and lamellar structures[13–15] have been generated by spin-coating or dip-coating, and various structures including a pancake-like morphology, strand-like aggregates, planar structure, and cellular patterns have been obtained at the air/liquid interface.[16–18]

Liquid/liquid interfaces that have different microenvironments from solutions and air/water interfaces have been utilized extensively to prepare inorganic nanoparticles,[19–23] to fabricate nanoparticulate films,[24–26] coordination polymer structures,[27–29] and polymer-based composite films.[30–37] Du and his coworkers investigated interfacial assembly of amphiphilic multiblock copolymer-capped noble metal nanoparticles at the liquid/liquid interface.[38] However, studies on the self-assembly behavior of block copolymers at the liquid/liquid interface are very rare.[39] In recent years, we have systematically investigated the adsorption and assembly of amphiphilic block copolymers at the liquid/liquid interface between two immiscible liquids. We found that amphiphilic block copolymers also exhibited abundant self-assembly behavior, whereby various nano- and microstructures, including foams, honeycomb-like and network structures, and even ordered arrays of nanospheres were formed.[40–42]

We subsequently developed this liquid/liquid interface adsorption and self-assembly method to fabricate microstructures of the amphiphilic block copolymer polystyrene-*b*-poly(acrylic acid)-*b*-polystyrene (PS-*b*-PAA-*b*-PS) with metal ions by using a mixed DMF/$CHCl_3$ solution as the organic phase instead of a $CHCl_3$ solution.[43,44] The DMF was found to migrate to the aqueous phase while the aqueous solution migrated to the organic phase across the interface immediately after the formation of the interface between the mixed solution and the aqueous solution containing the metal ions, resulting in the formation of W/O emulsions in the original organic solution due to the "ouzo effect".[45,46] The polymer molecules and metal ions adsorbed around the emulsion droplets and coordinated with each other, after which the fabricated emulsion droplets adsorbed and accumulated at the planar liquid/liquid interface, by further assembling into composite thin films with foam structures. This fabrication process is unique and different from the process that occurs at the interface between two kinds of immiscible solutions.

[a]*Key Laboratory for Colloid and Interface Chemistry of Education Ministry, Shandong University, Jinan 250100, P. R. China. E-mail: hgliu@sdu.edu.cn*

[b]*Anastro Laboratory, Department of Chemistry, Changwon National University, Changwon 641-773, Korea*

We had originally intended to fabricate composite films of other block copolymers using this modified method; thus, a planar liquid/liquid interface was constructed using a DMF/$CHCl_3$ mixed solution of PB-*b*-P4VP and a $HAuCl_4$ aqueous solution. However, to our surprise we found that a freestanding thin film appeared at the air/water interface rather than at the liquid/liquid interface. This is a novel phenomenon that has not yet been observed. Therefore, this interesting phenomenon was further investigated and the results are presented here. Our intention is to develop it into a facile way to fabricate a greater variety of composite polymer thin films.

Experimental section

Materials

PB-*b*-P4VP with the M_n values of the two blocks of 104 000/12 000 (M_w/M_n = 1.03) was purchased from Polymer Source (Canada) and used as received. $HAuCl_4 \cdot 3H_2O$ (99.9+%) was purchased from Aldrich. Chloroform, which was obtained from Tianjin Guangcheng Chem. Co., is an analytical reagent containing 0.3–1.0% ethanol as a stabilizer. DMF (≥99.5%) was obtained from Sinopharm Chemical Reagent Co., Ltd. (Shanghai, China), and used as received. KBH_4 (≥97.0%) was obtained from Shanghai Zhanyun Chemical. Co. Ltd., and 4-nitroaniline (4-NA, ≥99.5%) was supplied by Tianjin Kemiou Chem. Reagent Co., Ltd. The water that was used was highly purified using a UP water purification system (UPHW-IV-90T, Chengdu China) with a resistivity ≥ 18.0 MΩ cm.

Preparation of composites

A certain amount of PB-*b*-P4VP was dissolved in chloroform, to which a certain amount of DMF was added to form a mixed polymer organic solution of 0.20 mg mL^{-1}. The volume ratio of the DMF to $CHCl_3$ was 3/7. The mixed solution became turbid as the volume ratio further increased, because DMF is a selective solvent for this polymer. An aqueous solution of $HAuCl_4$ with a concentration of 1.0×10^{-3} mol L^{-1} was prepared by dissolving the salt in pure water.

About 5 mL of the polymer solution was poured into a clean and dry bottle with a diameter of 3.5 cm, and then a pipet was used to add 5 mL $HAuCl_4$ aqueous solution slowly and carefully along the bottle wall to cover the organic solution. A planar liquid/liquid interface was formed. The organic and aqueous phases are referred to as the lower and upper phases, respectively. Mass transfer was observed to take place across the interface as soon as the liquid/liquid interface had formed. The interface became unclear, a thin film formed rapidly at the air/liquid interface, and the liquid/liquid interface dropped to a lower level. The beaker was placed in a closed container in a dark oven. Twelve hours later, the film was deposited on solid substrates, such as carbon-coated copper grids, quartz slides and mica plates for further treatment and characterization.

Characterization

The morphology and structure of the deposited films were investigated using a high-resolution transmission electron microscope (HRTEM, JEOL-2010) with an accelerating voltage of 200 kV and an atomic force microscope (AFM, Nanoscope IIIa, Digital Instruments Inc.). The structure of the film was further confirmed using a SAXSess MC2 high flux small-angle X-ray scattering instrument (Anton Paar, Austrian) with a Ni-filtered Cu Kα radiation (0.154 nm), operating at 40 kV and 50 mA. The film compositions were probed by an X-ray photoelectron spectroscope (XPS, ESCALAB MKII) with an Mg Kα excitation source at a pressure of 1.0×10^{-6} Pa and a resolution of 1.00 eV.

In order to get the yield of the film, 50 mL of the polymer solution was used to form the film at the air/liquid interface using the method described above. All the film was deposited on a quartz slide and measured after drying by using an electronic balance (BT 25 S, Sartorius) with the sensitivity of 0.01 mg. The mass of the films was measured to be 0.25 mg. The yield was calculated to be 2.5%.

Catalytic reaction

The catalytic activities of the thin composite films were evaluated by using the reduction of 4-NA in aqueous solutions as a model reaction. A 0.5 mL aqueous solution of 4-NA with a concentration of 2×10^{-4} mol L^{-1} was poured into a 1 cm quartz cuvette, to which 1.0 mL of an aqueous solution of KBH_4 with a concentration of 2×10^{-2} mol L^{-1} was added. The final concentrations of 4-NA and KBH_4 in the mixture were 6.67×10^{-5} and 1.33×10^{-2} mol L^{-1}, respectively. The thin composite film was deposited on a quartz slide and treated with KBH_4 aqueous solution before it was immersed in the reaction system to catalyze the reduction of 4-NA. The progress of the reaction was monitored by using UV-vis spectroscopy (HP8453). The reaction temperature was controlled to be 30 °C by using a thermostat.

Results and discussion

Morphology and structure

The morphology and structure of the thin film formed at the air/liquid interface were investigated using TEM, as shown in Fig. 1. As seen in Fig. 1a and d, two kinds of sheet structures existed in the films: the first consists of large compact sheets with a size approximating tens of micrometers, whereas the other structure contains small sheets measuring several micrometers. The appearance of wrinkles indicated that these sheets overlapped in the film. From the high-magnification images (Fig. 1b and e), one can see that the Au nanoparticles were distributed homogeneously in both of the sheets. The mean diameter of the nanoparticles in the two respective sheets was measured to be 1.99 ± 0.57 and 2.03 ± 0.44 nm from Fig. 1c and f, respectively, which is very close to each other.

Fig. 2 shows the AFM images of the composite structure formed at the air/liquid interface. From Fig. 2a and b we can see many small sheets with a size of several tens of nanometers dispersed in a larger sheet. The thickness of the small sheets was measured to be 4.14 nm. It can be seen from Fig. 2c that the film has a stepped structure. The thickness between the two labels was derived to be 25.3 nm. Please note that the height

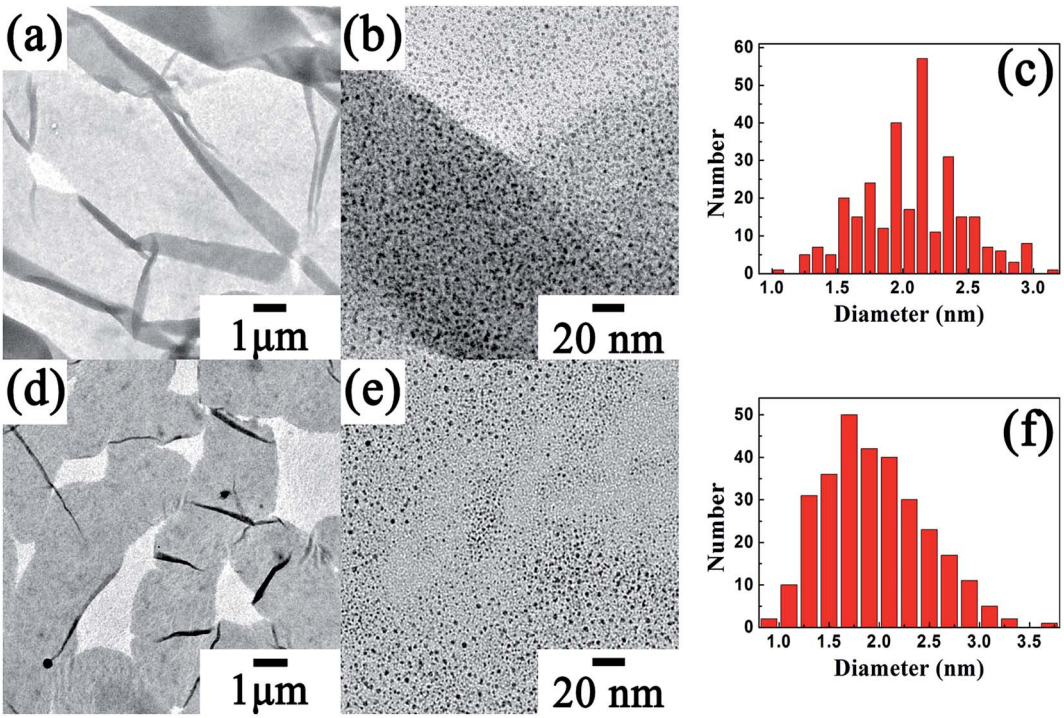

Fig. 1 TEM micrographs of PB-*b*-P4VP/Au composite film formed at the air/liquid interface (a, b, d and e), and the corresponding size distribution histograms (c and f) of the nanoparticles.

seems to exceed 200 nm, as shown in Fig. 2d, which was attributed to upward warping of the sheet edge. Fig. 2e shows the enlarged image of Fig. 2c, which shows clearly that the step is made up of six layers, indicating that the film has a multilayer structure. The thickness of one layer can be calculated to be 4.22 nm, close to the thickness of the smaller sheets in Fig. 2a. Fig. 2f also shows the layered structure of the film.

The film structure was further characterized by SAXS, as shown in Fig. 3. Four main diffraction bands appeared. The *d* values were calculated to be 7.70, 6.28, 4.28 and 3.37 Å, respectively. It is known that both PB and P4VP are non-crystalline polymers. So these diffraction bands should be attributed to the special film structure, *i.e.* the multilayered structures. They should be correspondence to the multilevel diffraction.

Formation mechanism

Fig. 4 shows the TEM micrographs of the aggregates formed in the original organic solution and the upper phase after the formation of the planar liquid/liquid interface. Small sheets with a size of about several tens of nanometers initially appeared, as in Fig. 4a, indicating that the aggregates were generated in the organic phase. These aggregates should be disk-like micelles that formed through self-assembly of the PB-*b*-P4VP molecules due to the poor solubility of the polymer in DMF and microphase separation of the polymer. Amphiphilic block copolymers are known to be capable of forming various organized molecular assemblies in solutions, including spherical and rod-like micelles, vesicles and lamellar structures, which are usually related to the critical packing parameter *p*. It should be noted that the length of the PB block in the polymer used here is much longer than that of the P4VP block. The PB blocks are intertwined, whereas the P4VP blocks extend freely into the solvent in the mixed solution. If these two blocks were to have a similar length, the *p* value would be sufficiently small, in which case spherical or rod-like micelles would form. However, the longer PB block increases the volume of the micellar core, leading to an increase in the value of *p* and the formation of the disk-like micelles. Here it is noteworthy that the size of these sheets approximates that of the smaller sheets appearing in Fig. 2a, indicating that the latter had its origins in the former. The large sheets with a size of about several tens of micrometers only appeared later, as shown in Fig. 4b–d, meaning that the larger sheet aggregates were generated in the upper phase after the formation of the liquid/liquid interface. It can be seen from Fig. 4b and c that some sheets have straight sides and cracks. The appearance of the cracks could be due to the shrinkage of the sheets after drying. These sheets arranged themselves by stacking up to form a multilayer structure, as is clearly shown in Fig. 4d. The particles adhered to the sides of the sheets and in the cracks should be related to the reduction of $AuCl_4^-$ ions in the aqueous solution by copper through galvanic reaction. It is clear that the multilayer films formed at the air/liquid interface have their origins in the aggregation of these sheets.

Based on the results above, a plausible formation process of the multilayer film at the air/liquid interface was proposed and is illustrated in Fig. 5. As soon as the liquid/liquid interface formed, the DMF carrying the PB-*b*-P4VP molecules, the small

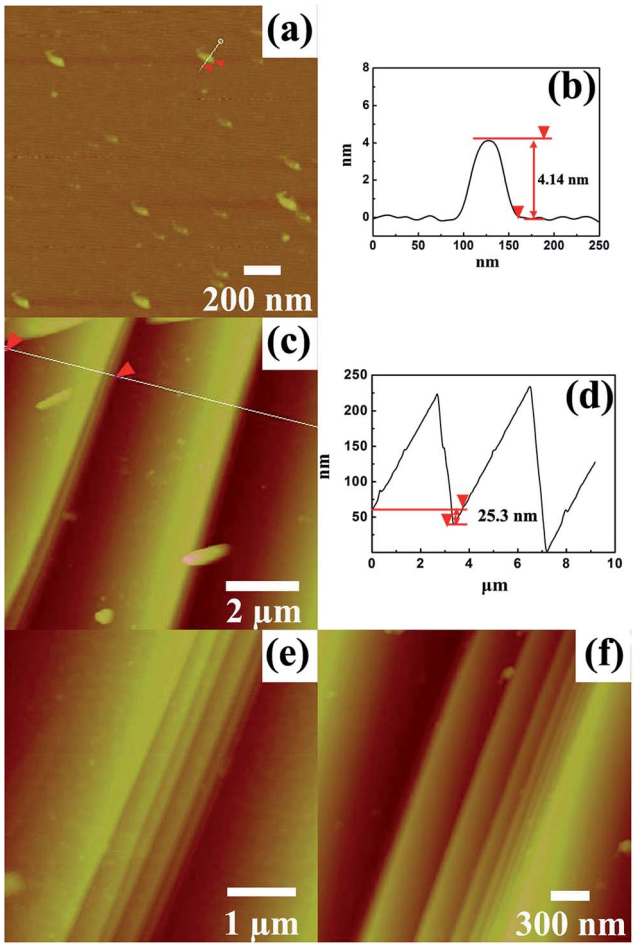

Fig. 2 AFM images (a, c, e and f) of the composite thin film of PB-*b*-P4VP/Au formed at the air/liquid interface. The line profiles (b) and (d) correspond to the images (a) and (c), respectively. The image (e) was obtained by scanning the labeled area in the image (c).

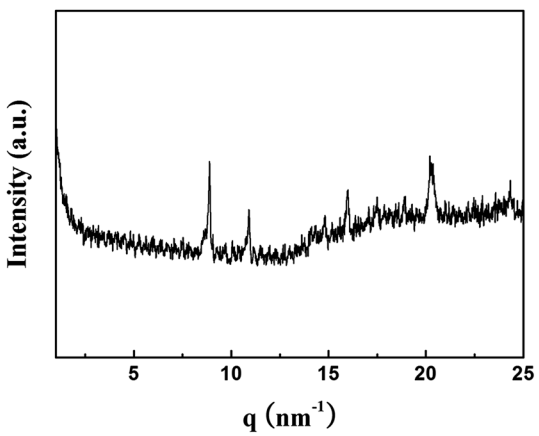

Fig. 3 SAXS pattern of the composite thin film of PB-*b*-P4VP/Au formed at the air/liquid interface.

sheets that formed in the mixed organic solution, and a small amount of $CHCl_3$, migrated across the interface into the aqueous phase due to the miscibility of DMF and water, leading

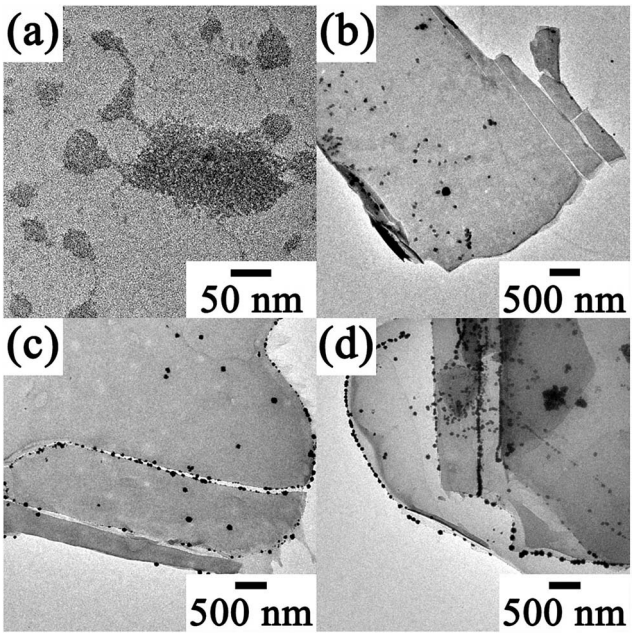

Fig. 4 TEM micrographs of the aggregates formed in the original organic phase (a) and in the upper phase (b–d) after the formation of the planar liquid/liquid interface. The samples were prepared by dropping a small amount of the corresponding solutions onto carbon-coated copper grids. Then the drops were sucked dry using filter papers. The sample corresponding to image (a) was stained using phosphotungstic acid.

to the formation of an O/W emulsion in the upper phase, while the planar liquid/liquid interface receded to a lower level at the same time. The DMF molecules contained within the droplets were quickly diffused into the water phase due to the stronger miscibility of DMF and water, and some small sheets and molecules also dispersed into water, which produced a water/DMF dispersion of the polymer molecules and the small sheets. With diffusion of DMF into water, the droplets became flat, the adsorbed layer around the droplet contact with each other to form a larger sheet at last. This process was illustrated in Fig. 6. The thickness of the sheet was measured to be about 4 nm, which was contributed by the PB core and the two P4VP shell layers. The formation of the sheets could be attributed to the "ouzo effect".[47,48] The $AuCl_4^-$ ions were combined with the sheets due to the interaction between the $AuCl_4^-$ ions and the protonated pyridine groups. Some $AuCl_4^-$ ions were reduced by DMF during this process and Au nanoparticles were produced. Subsequently, these sheets, perhaps together with some polymer molecules, adsorbed at the air/liquid interface to form a thin layer to reduce the surface tension and the total energy of the system, as shown in Fig. 5. It was reported that even hydrophilic colloidal particles could adsorb at the air/liquid interface with a high desorption activation energy.[49] With time, an increasing number of sheets moved to the air/liquid interface to attach themselves tightly to the upper layer to finally form a multilayer structure, as illustrated in the AFM images of the film.

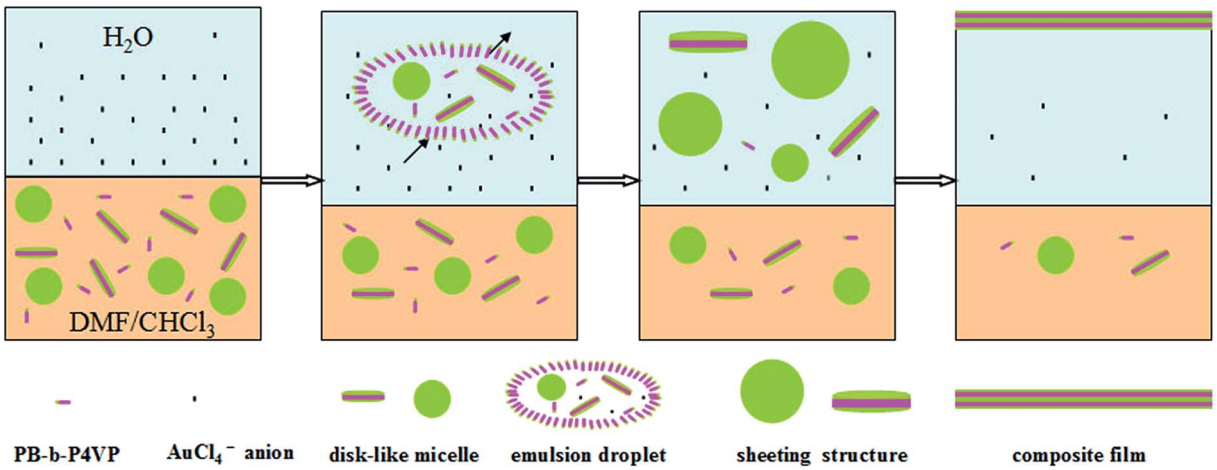

Fig. 5 Schematic representation of the formation process of the composite multilayer thin film at the air/liquid interface.

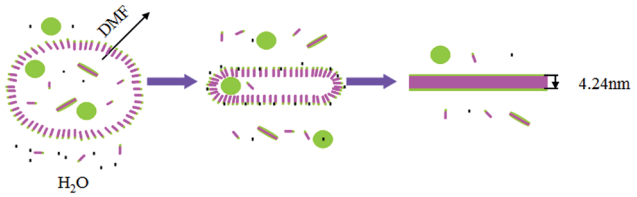

Fig. 6 Illustration of the formation of the larger sheet.

It seems somewhat strange that foam films formed at the liquid/liquid interface when using PS-*b*-PAA-*b*-PS[43,44] while a multilayer film formed at the air/liquid interface when using PB-*b*-P2VP under the similar conditions. This should be attributed to different molecular structures of the polymers. These polymers have different hydrophile–lipophile balance (HLB) values. In fact, the aqueous solution migrated into the organic phase and the DMF droplets migrated into the aqueous phase simultaneously, and the lower phases became turbid in the both cases. However, the lower phase became clear again in a short time when using PB-*b*-P2VP, because this polymer is more hydrophobic and can not stabilize the W/O emulsion droplets effectively. So no film formed at the liquid/liquid interface in this case. On the contrary, PS-*b*-PAA-*b*-PS has a moderate HLB value and can stabilize the emulsion droplets, resulting in the formation of foam films at the liquid/liquid interface. Both polymers self assembled into organized assemblies when transferred into the upper phases with DMF, as confirmed by the DLS observation.[44] However, no film was observed at the air/liquid interface for PS-*b*-PAA-*b*-PS, because the stronger hydrophilicity of the aggregates arising from the polar PAA blocks makes it difficult to adsorb at the interface. On the contrary, the aggregates formed by PB-*b*-PS are less hydrophilic and are easy to adsorb at the air/liquid interface to form a multilayer film.

A useful method has been developed to fabricate organized assemblies of amphiphilic block copolymer in aqueous solutions in recent years.[50–56] The block copolymer was dissolved in a small amount of a volatile organic solvent, such as chloroform and then dispersed in water to form a O/W emulsion. Molecular assemblies were produced during the evaporation of the organic solvent due to the interfacial instabilities. The method described in this paper is similar to but distinctly different from the solvent evaporation-driven method. Our method is a solvent diffusion-driven one in which the "ouzo effect" plays a crucial role both in the mass transfer from the lower phase to the upper phase and in the formation of the disk-like micelles. This is a unique technique to fabricate molecular assemblies of amphiphilic block copolymers and worth studying and extending in the future.

Two approaches, *i.e.* Langmuir monolayer and Gibbs adsorption technique have been applied to fabricate organized molecular assemblies of water insoluble amphiphiles and to study the adsorption and assembling behavior of surfactants at the air/water interface, respectively. PB-*b*-P2VP is an amphiphilic water insoluble block copolymer. However, with the aid of phase transfer, the polymer molecules and aggregates can be dispersed in a strong polar water/DMF medium and further adsorb at the air/liquid interface through the Gibbs adsorption route. Therefore, this method described here can be considered as a new and novel technique for the fabrication of molecular assemblies that differs from the traditional Langmuir monolayer and Gibbs adsorption technique.

In general, ordered multilayer films can be fabricated through the Langmuir–Blodgett (LB) technique or by a layer-by-layer (LbL) deposition method. Here, we provide a unique and facile method to prepare thin films with an ordered multilayer structure. Of course this method is not suitable for producing multilayer films of all materials, and could sometimes lead to the formation of thin films with alternative structures. Nevertheless, our method constitutes a new way of fabricating thin films.

Composition analysis

The composition of the composite film formed at the air/liquid interface was checked using XPS, as shown in Fig. 7. Two bands

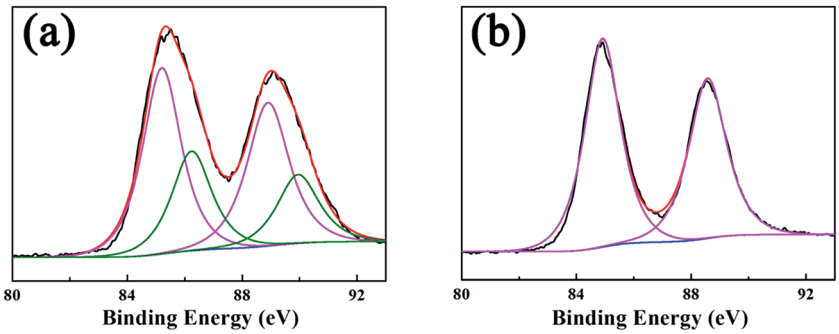

Fig. 7 XPS spectra of gold elements in the as-prepared composite film (a), and the film treated with an aqueous solution of KBH_4 (b).

appeared between 82 and 92 eV, corresponding to Au $4f_{7/2}$ and $4f_{5/2}$, respectively. In the spectrum of the as-prepared PB-*b*-P4VP/Au composite film shown in Fig. 7a, the bands were decomposed into two pairs of peaks. The first pair of peaks at 85.2/88.9 eV was assigned to $4f_{7/2}$ and $4f_{5/2}$ of the spin–orbit coupling of Au(0), which means that some $AuCl_4^-$ ions were reduced by DMF in the self-assembly process.[42] The binding energy of 85.2 eV is much greater than that of bulk Au(0),[57,58] indicating the formation of smaller gold nanoparticles in the composite film, because the binding energy of Au(0) increases with decreasing particle size.[59,60] This is consistent with the mean size of the nanoparticles shown in Fig. 1. The second pair of peaks at 86.3/90.0 eV was assigned to Au(III),[34] which was attributed to the presence of $AuCl_4^-$ ions. Based on the peak areas, the relative contents of Au(0) and Au(III) were calculated to be 65.5% and 35.5%, respectively. In the XPS spectrum of the composite film treated with an aqueous solution of KBH_4 (Fig. 7b), two symmetric peaks appeared at 84.9 and 88.6 eV, which correspond to $4f_{7/2}$ and $4f_{5/2}$ of Au(0),[42] respectively, indicating that almost all the $AuCl_4^-$ anions were reduced. The binding energy of 84.9 eV was slightly lower than 85.2 eV, the binding energy of Au(0) in the untreated film, but still much greater than that of bulk Au(0), indicating that there was no significant change in the size of the nanoparticles after further treatment.

Catalytic properties

The reduction of 4-NA by KBH_4 in aqueous solutions was used as a model reaction to evaluate the catalytic activity of the composite film.[61] The UV-vis spectra of the reaction system at different reaction times are shown in Fig. 8a. It can be seen that a new peak at 237 nm corresponding to *p*-phenylenediamine appeared while the absorption peak of 4-NA centered at 380 nm weakened gradually with time, indicating that 4-NA was reduced to *p*-phenylenediamine in the presence of the catalyst. This reaction was regarded as a pseudo-first-order reaction because the concentration of KBH_4 in the reaction system greatly exceeded that of 4-NA and was considered to be constant during the reaction process. The apparent rate constant (k_{app}) of the reaction can be obtained from the slope of the linear fitted line of $\ln(A_t/A_0) \sim t$, as shown in Fig. 8b. Fig. 8c provides the relationship between k_{app} and the number of reduction cycles. The uninterrupted use of the composite film as catalyst for 20 cycles, led to a gradual and obvious increase in k_{app} until the 16th cycle was reached, after which the rate constant stabilized until the 20th cycle. It was found that the k_{app} value of the 20th cycle was nearly five times that of the 1st cycle. After exposure to air for 10 hours, the film was reused to continuously catalyze the reaction from the 21th to 42th cycle. The variation of k_{app} with the reaction cycles was similar to what was observed during the first 20 cycles. This phenomenon was very strange and different from the literature results. In general, when a composite film is used as catalyst, k_{app} either remained constant or decreased with increasing reaction cycles, depending on the stability of the catalyst film. For example, we have prepared some polymer/noble metal nanoparticle composite porous films with a foam and honeycomb microstructure that exhibited nearly constant catalytic activities for the hydrogenation of nitro-compounds in aqueous solutions for several cycles.[35,36,42]

The unique catalytic feature of the PB-*b*-P4VP composite film was attributed to the compact multilayer structure in which catalytic Au nanoparticles were homogeneously incorporated. The catalytic reaction would not occur until the reactants diffused to the surface of the nanoparticles; thus, in this case the reaction rate is determined by the diffusion of the reactants. At first, when the dry film deposited on a glass slide was immersed in the reaction system, the film was wetted, and the reactants gradually diffused into the film with water, enabling the catalytic reaction to take place. As the immersion time increased, the diffusion rate was enhanced and the diffusion depth increased, enabling increasing numbers of Au nanoparticles to participate in the catalytic reaction, ultimately resulting in the increase of k_{app} with an increasing number of reaction cycles. When the porous composite films were used as catalysts, k_{app} remained nearly constant, because of the facile diffusion of the reactants into these films. After exposure to air for about 10 hours, the film became dry. Upon reuse of the film, k_{app} first increased and then became constant with increasing cycles. The k_{app} value of the 43th cycle is clearly higher than that of the 1st and the 21th cycles, respectively, even though the film was also exposed to air for 10 hours. This indicated that the path along which the reactants could diffuse remained open after the film was used many times. After the 58th cycle, the value of k_{app} decreased

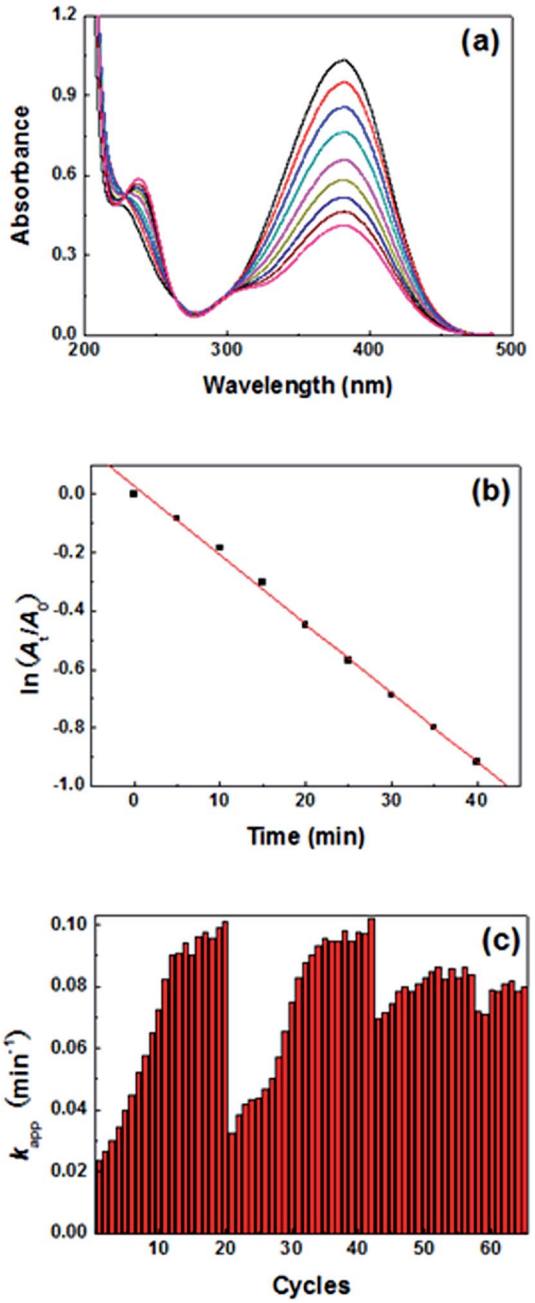

Fig. 8 Catalytic reduction of 4-NA: (a) time-dependent absorption spectra of the reaction solution in the presence of the PB-*b*-P4VP/Au composite thin film. (b) Plot of $\ln(A_t/A_0)$ against the reaction time. (c) Relationship between the reaction rate constants and the number of reduction cycles. The reaction temperature is 303 K.

slightly, because the film was exposed to air for a short time (about half an hour). This indicated that the wetting state of the film has an important effect on the catalytic efficiency. Hariprasad and Radhakrishnan have investigated the catalytic behavior of a multilayer film of poly(vinyl alcohol)/Ag–poly(vinyl alcohol)–poly(vinyl alcohol)/Ag in an aqueous medium.[62] They found that the polymer matrix swelling in the aqueous medium played a crucial role in channeling the reactants to the catalyst and the products away. It is possible that the PB-*b*-P2VP/Au composite film swells in the aqueous medium and allows the reactants to diffuse into the film.

Conclusions

A multilayer composite thin film that formed at the air/liquid interface was fabricated using a new and facile way *via* phase transfer, self-assembly, and adsorption steps. The composite thin film of PB-*b*-P4VP doped with Au nanoparticles was found to exhibit unique heterogeneous catalytic properties for the reduction of 4-NA by KBH_4 in aqueous solutions. This method can also be used to achieve the self-assembly of other polymers with different functional inorganic or organic species, thereby paving the way for a new method for the fabrication of composite films in nanotechnology applications.

Acknowledgements

This work was supported by grants from the National Natural Science Foundation of China (No. 21273133).

Notes and references

1 R. J. Hickey, A. S. Haynes, J. M. Kikkawa and S.-J. Park, *J. Am. Chem. Soc.*, 2011, **133**, 1517–1525.
2 X. Wang, M. Goswami, R. Kumar, B. G. Sumpter and J. Mays, *Soft Matter*, 2012, **8**, 3036–3052.
3 S. E. Mastroianni and T. H. Epps III, *Langmuir*, 2013, **29**, 3864–3878.
4 M. Luo and T. H. Epps III, *Macromolecules*, 2013, **46**, 7567–7579.
5 J. Y. Park and R. C. Advincula, *Soft Matter*, 2011, **7**, 9829–9843.
6 L. Zhao and Z. Lin, *Soft Matter*, 2011, **7**, 10520–10535.
7 G. Rizis, T. G. M. van de Ven and A. Eisenberg, *Angew. Chem., Int. Ed.*, 2014, **53**, 9000–9003.
8 Y. Shi, W. Zhu, D. Yao, M. Long, B. Peng, K. Zhang and Y. Chen, *ACS Macro Lett.*, 2014, **3**, 70–73.
9 I. C. Riegel, D. Samios, C. L. Petzhold and A. Eisenberg, *Polymer*, 2003, **44**, 2117–2128.
10 Y. Mai and A. Eisenberg, *Chem. Soc. Rev.*, 2012, **41**, 5969–5985.
11 L. Wang, H. Huang and T. He, *Macromol. Rapid Commun.*, 2014, **35**, 1387–1396.
12 H. Park, J.-U. Kim and S. Park, *Nanoscale*, 2012, **4**, 1362–1367.
13 D. Ahn and E. Sancaktar, *Soft Matter*, 2008, **4**, 1454–1466.
14 Y. Lu, H. Xia, G. Zhang and C. Wu, *J. Mater. Chem.*, 2009, **19**, 5952–5955.
15 K. G. Yager, E. Lai and C. T. Black, *ACS Nano*, 2014, **8**, 10582–10588.
16 G. Wen, B. Chung and T. Chang, *Polymer*, 2006, **47**, 8575–8582.
17 E. W. Price and Y. Guo, *Langmuir*, 2009, **25**, 6398–6406.
18 J. K. Cox, K. Yu, B. Constantine, A. Eisenberg and R. B. Lennox, *Langmuir*, 1999, **15**, 7714–7718.

19 C. N. R. Rao, G. U. Kulkarni, P. J. Thomas, V. V. Agrawal and P. Saravanan, *J. Phys. Chem. B*, 2003, **107**, 7391–7395.
20 L. Zheng and L. Li, *J. Phys. Chem. B*, 2005, **109**, 1108–1112.
21 T. Kida, *Langmuir*, 2008, **24**, 7648–7650.
22 X. Song, S. Sun, W. Zhang, H. Yu and W. Fan, *J. Phys. Chem. B*, 2004, **108**, 5200–5205.
23 S. J. Hoseini, M. Bahrami and M. Roushani, *RSC Adv.*, 2014, **4**, 46992–46999.
24 M. Gadogbe, S. M. Ansar, I.-W. Chu, S. Zou and D. Zhang, *Langmuir*, 2014, **30**, 11520–11527.
25 H. Duan, D. Wang, D. G. Kurth and H. Mohwald, *Angew. Chem., Int. Ed.*, 2004, **43**, 5639–5642.
26 K. Y. Lee, G.-W. Cheong and S. W. Han, *Colloids Surf., A*, 2006, **275**, 79–82.
27 B. Liu, D.-J. Qian, H.-X. Huang, T. Wakayama, S. Hara, W. Huang, C. Nakamura and J. Miyake, *Langmuir*, 2005, **21**, 5079–5084.
28 B. Liu, D.-J. Qian, M. Chen, T. Wakayama, C. Nakamura and J. Miyake, *Chem. Commun.*, 2006, 3175–3177.
29 Y. Tang, H.-T. Wang, M. Chen, D.-J. Qian, L. Zhang and M. Liu, *Nanoscale Res. Lett.*, 2014, **9**, 488.
30 J. J. Benkoski, S. E. Bowles, B. D. Korth, R. L. Jones, J. F. Douglas, A. Karim and J. Pyun, *J. Am. Chem. Soc.*, 2007, **129**, 6291–6297.
31 S. Yang, C.-F. Wang and S. Chen, *J. Am. Chem. Soc.*, 2011, **133**, 8412–8415.
32 C. Zhou, N. Chen, J. Yang, H. Liu and Y. Li, *Macromol. Rapid Commun.*, 2012, **33**, 688–692.
33 D. B. Carew, K. J. Channon, I. Manners and D. N. Woolfson, *Soft Matter*, 2011, **7**, 3475–3481.
34 L.-J. Chen, H. Ma, K. Chen, H.-R. Cha, Y.-I. Lee, D.-J. Qian, J. Hao and H.-G. Liu, *J. Colloid Interface Sci.*, 2011, **362**, 81–88.
35 H. Ma, Y. Geng, Y.-I. Lee, J. Hao and H.-G. Liu, *J. Colloid Interface Sci.*, 2013, **394**, 223–230.
36 L. Lin, K. Shang, X. Xu, C. Chu, H. Ma, Y.-I. Lee, J. Hao and H.-G. Liu, *J. Phys. Chem. B*, 2011, **115**, 11113–11118.
37 Y.-G. He, S.-Y. Shi, N. Liu, Y.-Y. Zhu, Y.-S. Ding, J. Yin and Z.-Q. Wu, *RSC Adv.*, 2015, **5**, 39697–39704.
38 B. Du, X. Chen, B. Zhao, A. Mei, Q. Wang, J. Xu and Z. Fan, *Nanoscale*, 2010, **2**, 1684–1689.
39 Z. Sun, T. Feng and T. P. Russell, *Langmuir*, 2013, **29**, 13407–13413.
40 D. Wang, H. Ma, C. Chu, J. Hao and H.-G. Liu, *J. Colloid Interface Sci.*, 2013, **402**, 75–85.
41 M. Liu, Y. Geng, Q. Wang, Y.-I. Lee, J. Hao and H.-G. Liu, *RSC Adv.*, 2015, **5**, 4334–4342.
42 Y. Liu, L. Chen, Y. Geng, Y.-I. Lee, J. Hao and H.-G. Liu, *J. Colloid Interface Sci.*, 2013, **407**, 225–235.
43 M. Liu, Q. Wang, Y. Geng, C. Wang, Y.-I. Lee, J. Hao and H.-G. Liu, *Langmuir*, 2014, **30**, 10503–10512.
44 Y. Geng, M. Liu, K. Tong, J. Xu, Y.-I. Lee, J. Hao and H.-G. Liu, *Langmuir*, 2014, **30**, 2178–2187.
45 M. Kowacz, J. M. S. S. Esperança and L. P. N. Rebelo, *Soft Matter*, 2014, **10**, 3798–3805.
46 N. L. Sitnikova, R. Sprik and G. Wegdam, *Langmuir*, 2005, **21**, 7083–7089.
47 P. Lucas, M. Vaysse, J. Aubry, D. Mariot, R. Sonnier and F. Ganachaud, *Soft Matter*, 2011, **7**, 5528–5531.
48 H. Fan and Z. Jin, *Soft Matter*, 2014, **10**, 2848–2855.
49 J.-W. Hu, G.-B. Han, B. Ren, S.-G. Sun and Z.-Q. Tian, *Langmuir*, 2004, **20**, 8831–8838.
50 Y. Geng and D. E. Discher, *J. Am. Chem. Soc.*, 2005, **127**, 12780–12781.
51 Y. Geng and D. E. Discher, *Polymer*, 2006, **47**, 2519–2525.
52 J. Zhu and R. C. Hayward, *J. Am. Chem. Soc.*, 2008, **130**, 7496–7502.
53 J. Bae, J. Lawrence, C. Miesch, A. Ribbe, W. Li, T. Emrick, J. Zhu and R. C. Hayward, *Adv. Mater.*, 2012, **24**, 2735–2741.
54 S. G. Jang, D. J. Audus, D. Klinger, D. V. Krogstad, B. J. Kim, A. Cameron, S.-W. Kim, K. T. Delaney, S.-M. Hur, K. L. Killops, G. H. Fredrickson, E. J. Kramer and C. J. Hawker, *J. Am. Chem. Soc.*, 2013, **135**, 6649–6657.
55 M. Su and Z. Su, *Macromolecules*, 2014, **47**, 1428–1432.
56 X. Nie, J. Cui and W. Jiang, *Soft Matter*, 2014, **10**, 8051–8059.
57 K. Kishi and S. Ikeda, *J. Phys. Chem.*, 1974, **78**, 107–112.
58 J. R. Mycroft, G. M. Bancroft, N. S. McIntyre and J. W. Lorimer, *Geochim. Cosmochim. Acta*, 1995, **59**, 3351–3365.
59 Y. L. Mikhlin, A. S. Romanchenko and I. P. Asanov, *Geochim. Cosmochim. Acta*, 2006, **70**, 4874–4888.
60 H.-L. Zhang, S. D. Evans, J. R. Henderson, R. E. Miles and T. Shen, *J. Phys. Chem. B*, 2003, **107**, 6087–6095.
61 H. Jia, X. Gao, Z. Chen, G. Liu, X. Zhang, H. Yan, H. Zhou and L. Zheng, *CrystEngComm*, 2012, **14**, 7600–7606.
62 E. Hariprasad and T. P. Radhakrishnan, *Chem.–Eur. J.*, 2010, **16**, 14378–14384.